EFFECT OF SHELL ON PERFORMANCE OF HEAT EXCHANGER WITH TREFOIL-HOLE BAFFLE

by

Yingjia WANG[a*], Qingfei DU[b], Xingchen LI[c], Minshan LIU[c], and Zunchao LIU[c*]

[a] School of Mechanical Engineering,
North China University of Water Resources and Electric Power, Zhengzhou City, China
[b] Henan Province Investment Intelligent Energy Ltd, Zhengzhou City, China
[c] School of Mechanics and Safety Engineering, Zhengzhou University, Zhengzhou City, China

Original scientific paper
https://doi.org/10.2298/TSCI211106028W

The periodic whole cross-section model and the periodic unit duct model were established, and the differences between two models were discussed. The effects of shell wall and baffle edges on the shell side performance of the heat exchanger with trefoil-hole baffle were investigated using both models. Thermodynamics in the shell side and heat transfer coefficient of each tube in different position were discussed. It is found that disparities between the results of the two numerical models decreases with the increase of the inner shell diameter. When the shell diameter is 0.8 m, the disparity is less than 10%, which means that the effects of the shell wall and the edges of baffles become weaker. When the shell diameter is less than 0.8 m, modified correlations for the periodic unit duct model are introduced to quantitatively reveal the effects of shell wall and baffle edges on thermodynamics with the variations of the shell diameter and baffle spacing. The fluid-flow velocities at specific locations on the shell side were measured using a laser doppler velocimeter system. The accuracy of the numerical simulation method was verified by the experimental results.

Key words: *heat exchanger, CFD, numerical model, trefoil-hole baffle, periodic whole cross-section model, periodic unit duct model*

Introduction

Shell and tube heat exchangers (STHX) have been widely adopted in engineering practices [1, 2]. Along with economy and society development, energy saving and emission reduction has become one of the hot issues in the modern scientific community [3], and the structures of STHX have also been improved a lot [4]. Different novel STHX have been presented successfully and developed gradually [5], such as trefoil-hole baffle [6], helical baffle [7, 8], staggered baffle [9], shutter baffle [10], corrugated tube [11], louver baffle [12] and so on.

The CFD is helpful for studying fluid-flow and heat transfer, designing a heat exchanger system as well as in trouble shooting or optimization [13]. By using CFD technology, various problems and their solutions encountered in the heat exchangers have been carried out. The thermo-hydraulic performance of the STHX with different baffle types was extensively evaluated [14-17]. Turbulence models were assessed for temperature predictions [18]. To im-

* Corresponding authors, e-mail: wangyingjia@ncwu.edu.cn, zchliu@zzu.edu.cn

prove heat transfer efficiency and reduce costs, the structure of the heat exchanger is usually optimized [19].

In a pressurized water reactor nuclear power plant, heat exchangers with trefoil-hole baffles are the main heat transfer equipment [20]. On the shell side, the tubes are supported by trefoil-hole baffles [6]. A jet is generated in the void between the edge of the orifice and the tube wall. The jets scour the surface of the tubes, which thins the boundary-layer thickness and improves the heat transfer efficiency [20]. With this flow pattern, the stagnant zones and the flow induced vibration in shell side are reduced. Moreover, heat exchanger with longitudinal fluid-flow in shell side is able to avoid tube bundle vibration very well [21, 22], and obtain a heat transfer coefficient 10% higher than that of the STHX with segmental and helical baffles [22]. Numerical simulation was used to study the thermohydraulic performances and mechanism of the shell side of heat exchanger with trefoil-hole baffles [6, 23]. Performances of heat exchangers with trefoil-hole baffles and quatrefoil-hole baffles were studied [24].

In the numerical investigation of STHX, it is crucial to build an appropriate numerical model. There are four typical models commonly used in current numerical simulations of STHX, which are unit model, periodic model, porous model, and whole model [25-27]. In the shell-side configuration, the geometry changes repeatedly along the flow direction, resulting in a periodically fully developed flow pattern [28]. The periodic whole cross-section model (PWCM) and periodic unit duct model (PUDM) are adopted usually in the study on performances of the shell side for the heat exchangers with longitudinal fluid-flow in shell side [29]. The PWCM includes the geometry structures of the shell wall and baffles, allowing the evaluation of their influence on the shell-side fluid-flow and heat transfer characteristics. But when shell diameter is large, a large number of grids is needed, which substantially increases the computer resources needed to carry out the calculations [30, 31]. The PUDM is only related to the tube lay-out and baffles, so the model is not limited by the shell diameter and the number of tubes [32]. Overall, extensive numerical studies have been done to analyze thermodynamics in the shell-side of the STHX with different geometric structures, but the specific applicability, the detailed difference, and the cause factors for two numerical models are still not clear. It is of great significance to evaluate the effect of the shell wall and the edges of the baffles on results, to discuss the difference between the two numerical models applying to the same structure, and to analyze the applicability of the models. The 3-D numerical models of the heat exchanger with trefoil-hole baffles were built and analyzed using FLUENT. Thermodynamics in the shell side and heat transfer coefficient of each tube in different position were discussed, and the shell wall and baffles edges on the characteristics of fluid-flow and heat transfer in the shell side were analyzed. By comparing the numerical simulation results of the two models, modified correlations for the PUDM are fitted. The accuracy of the numerical simulation results was verified by fluid-flow experiments.

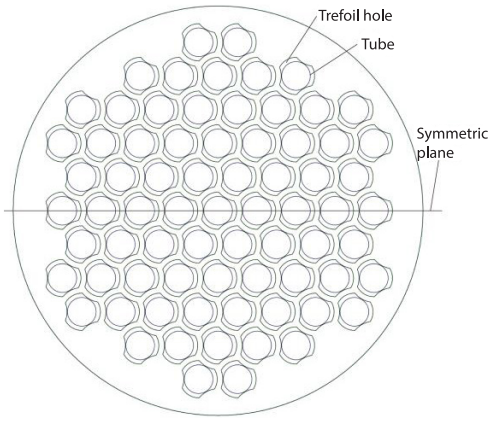

Figure 1. Arrangement of trefoil holes in the baffle

Numerical model and calculation

Physical model and method

A PWCM and a PUDM for the shell side of a heat exchanger with trefoil-hole baffles were developed. The arrangement of trefoil

holes in the baffle is shown in fig. 1, and the main geometrical parameters of the heat exchanger are listed in tab. 1. Considering the geometric symmetry, the model can be built with a symmetric boundary condition, as shown in fig. 2(a). A PUDM is built with three tubes, but without consideration of the shell wall, as shown in fig. 2(b). In the two models, the two end faces of the models are set as periodic conditions. The walls of shells and baffles were set as non-slip boundary conditions and the mass-flow rate in the shell side was inputted. The symmetric plane in the PWCM and the planes adjacent to tubes are all set as symmetric conditions.

Table 1. Geometrical dimensions of computation models

Heat transfer tube [m]	Tube pitch [m]	Arrangement of tubes	Height of trefoil holes [m]	Thickness of baffle [m]	Baffle spacing [m]
$\Phi 0.014 \times 0.001$	0.019	Orthogonal triangle	0.0023	0.01	0.15, 0.3, 0.6

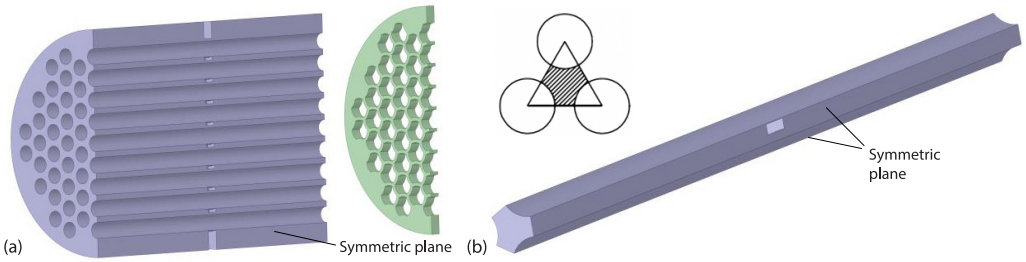

Figure 2. Sketches of the numerical periodic models; (a) PWCM and (b) PUDM

The model is divided into several regular parts using GAMBIT software, and the individual parts are meshed using a structured grid. The mesh is refined near the trefoil-hole baffle. The quality of the obtained grid is good. The grid-independence is verified by using the heat transfer coefficient and pressure drop as criteria. The grid is gradually refined and the relative error between the results obtained from the current grid and the last grid before refinement is calculated, and when it is less than 1%, the obtained solution is considered to be grid independent. The grids number of the two models after the grid independence verification is 265000 and 3286000. It is verified that more than 95% of the near-wall nodes have a $Y+$ value less than 1. The standard k-ε turbulence model with energy equations is chosen for the numerical simulation, and the enhanced wall function is used. The SIMPLE algorithm is used for the coupling of pressure and velocity. The second-order upwind format is used for both momentum and energy discretization. Referring to the actual structural dimensions of the heat exchanger with trefoil-hole baffles for nuclear power, the operating conditions are used as the boundary conditions for the numerical simulation, and several assumptions are made:

– Assuming that the medium in the heat exchanger tube side is excess saturated steam, so the wall surface of the heat exchanger tube is a constant wall temperature boundary condition, and the temperature is set to 393 K. The shell side medium is water, and the flow direction are along the axial direction of the heat exchanger tube.
– In the fully developed section of the shell side, the flow and heat transfer of the fluid are periodic, so the model inlet and outlet are set as periodic boundary conditions with given mass-flow rate and fluid temperature of 308 K. The symmetric plane is set as a symmetric boundary condition.

– In actual engineering applications, the shell outer wall of the heat exchanger is equipped with an insulation layer, so the outer wall surface of the shell is set as an adiabatic boundary condition.

Governing equations

The governing equations in the numerical calculation are as follows [33, 34]. Equations (1)-(3) are the continuity equation, the momentum equation, and the energy equation, respectively:

$$\frac{\partial u}{\partial x}+\frac{\partial v}{\partial y}+\frac{\partial w}{\partial z}=0 \tag{1}$$

$$\begin{aligned}\rho\left(u\frac{\partial u}{\partial x}+v\frac{\partial u}{\partial y}+w\frac{\partial u}{\partial z}\right)&=-\frac{\partial p}{\partial x}+\mu\left(\frac{\partial^2 u}{\partial x^2}+\frac{\partial^2 u}{\partial y^2}+\frac{\partial^2 u}{\partial z^2}\right)\\ \rho\left(u\frac{\partial v}{\partial x}+v\frac{\partial v}{\partial y}+w\frac{\partial v}{\partial z}\right)&=-\frac{\partial p}{\partial y}+\mu\left(\frac{\partial^2 v}{\partial x^2}+\frac{\partial^2 v}{\partial y^2}+\frac{\partial^2 v}{\partial z^2}\right)\\ \rho\left(u\frac{\partial w}{\partial x}+v\frac{\partial w}{\partial y}+w\frac{\partial w}{\partial z}\right)&=-\frac{\partial p}{\partial z}+\mu\left(\frac{\partial^2 w}{\partial x^2}+\frac{\partial^2 w}{\partial y^2}+\frac{\partial^2 w}{\partial z^2}\right)\end{aligned} \tag{2}$$

$$\rho c_p\left(u\frac{\partial T}{\partial x}+v\frac{\partial T}{\partial y}+w\frac{\partial T}{\partial z}\right)=\lambda\left(\frac{\partial^2 T}{\partial x^2}+\frac{\partial^2 T}{\partial y^2}+\frac{\partial^2 T}{\partial z^2}\right) \tag{3}$$

where u, v, and w are velocity components in the Cartesian co-ordinate system, x, y, and z are co-ordinates in the Cartesian co-ordinate system, ρ – the fluid density p – the pressure, μ – the dynamic viscosity, c_p – the specific heat capacity, T – the temperature, and λ – the thermal conductivity.

The fully developed periodic fluid-flow has the following periodic boundary conditions [32]:

$$\begin{aligned}u(x,y,z)&=u(x,y,z+s)\\ v(x,y,z)&=v(x,y,z+s)\\ w(x,y,z)&=w(x,y,z+s)\end{aligned} \tag{4}$$

$$p(x,y,z)-p(x,y,z+s)=p(x,y,z+s)-p(x,y,z+2s) \tag{5}$$

where s is model length in periodic model.

The pressure drop is represented by a pressure gradient [25], which is defined:

$$\Delta p=\frac{p(x,y,z)-p(x,y,z+s)}{s} \tag{6}$$

Validation of numerical model

To verify the validity and accuracy of the numerical models and methods used in this paper, an experiment of fluid-flow in the shell side of heat exchanger with trefoil-hole baffle was carried out. A laser doppler velocimeter (LDV) [35, 36] was used to measure the fluid velocity. The sketch of experiment test is shown in fig. 3(a). Based on geometric and operational parameters in the experiment, a PWCM was built, and calculations were carried out with the same methods described previously. The model diagram and the main structural parameters are

shown in the figs. 3(b) and 3(c). The velocities of several points on-line 1 were measured. The position of line 1 is shown in the fig. 3(c).

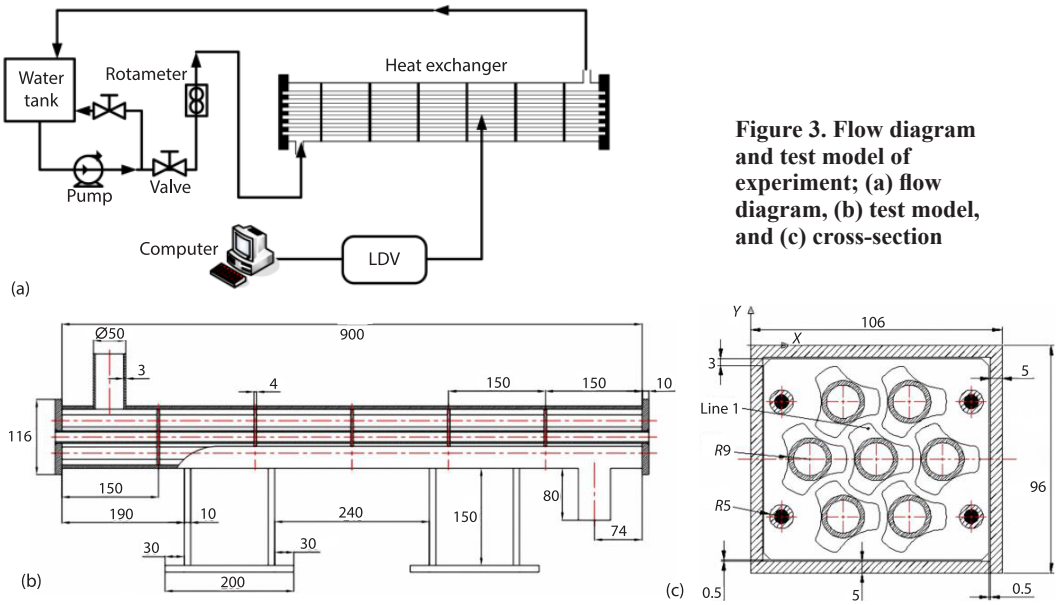

Figure 3. Flow diagram and test model of experiment; (a) flow diagram, (b) test model, and (c) cross-section

The accuracy of the experimental set-up depends mainly on the precision of the LDV system and the hydraulic measurement system. The error of fluid velocity measurements for the LDV system is less than 0.2%. With professional calibration, the error caused by mounting accuracy is less than 0.8% [24]. For the hydraulic measurement system, the uncertainty mainly comes from the volumetric flow rate obtained by the rotameter with an accuracy of 2.5%.

The comparison between measured results and the simulated results at the flow rate, Q, of 5.0 m^3/h is shown in fig. 4. The error between the measured and simulated values of the main flow velocity is mostly less than 15%. The following other factors may lead to deviations between experimental values and numerical results: manufacturing errors in the experimental model and errors in the location of the measurement points. It indicates that the numerical simulation method and numerical simulation results are reliable and accurate.

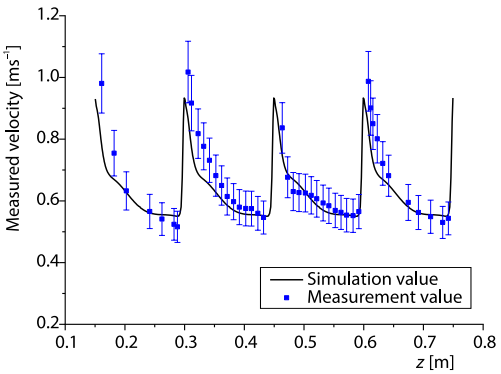

Figure 4. Comparison between experimental results and numerical results

Results and discussions

Difference between the two models

In the numerical calculations, the baffle spacings, L_b, were selected as 0.15 m, 0.3 m, and 0.6 m, respectively, and the shell diameters, D, were selected as 0.2 m, 0.3 m, 0.4 m, 0.5 m, 0.6 m, and 0.8 m, respectively. The mean velocity varies from 0.28 m/s to 2.33 m/s in the shell side, which corresponds to the Reynolds number range from 6000-50000. For the tube lay-out

considered in this paper, the hydraulic diameter, d_e, is calculated by the cross-sectional area and the wetted perimeter of the shaded area in fig. 2(b). The correlation for d_e and the shell side heat transfer coefficient, h, are [37]:

$$d_e = \frac{4\left(\frac{\sqrt{3}P_t^2}{2} - \frac{\pi d_o^{\,2}}{4}\right)}{\pi d_o} \tag{9}$$

$$h = \frac{\dot{m}c_p\left(T_{out} - T_{in}\right)}{A\left(T_w - T\right)} \tag{10}$$

where P_t is the tube pitch size, d_o – the tube outside diameter, $\dot{m}$ – the mass-flow rate, A – the heat transfer area, T – mean bulk temperature of fluid, T_w – the temperature of tube wall, T_{in} – mean temperature of inlet fluid, and T_{out} – the mean temperature of outlet fluid.

The variation of heat transfer coefficient and pressure drop with the shell diameter at different Reynolds numbers have similarities. The heat transfer coefficients and pressure gradients obtained by using the two models were compared with different shell diameters, D, baffle spacing, L_b, of 0.15 m, and Re = 10000, which are shown in fig. 5. The ratios of heat transfer coefficients, pressure drops and heat transfer coefficient per unit pressure drop obtained by the two models, h'/h, $\Delta p'/\Delta p$, and $(h'/\Delta p')/(h/\Delta p)$, changing with Reynolds numbers are compared in fig. 6.

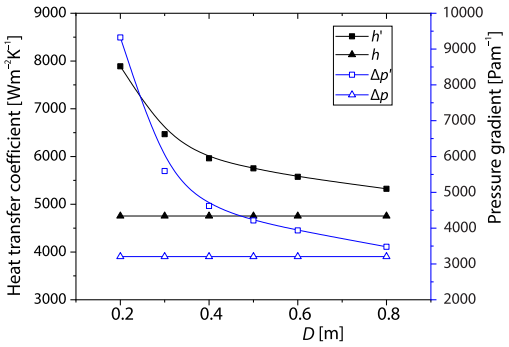

Figure 5. Comparison of the results obtained by two models when Re = 10000

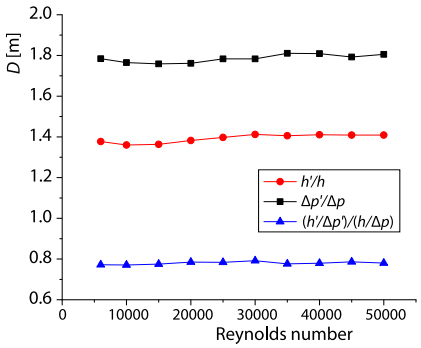

Figure 6. The h'/h, $\Delta p'/\Delta p$ and $(h'/\Delta p')/(h/\Delta p)$ *vs.* Reynolds number at shell diameter of 0.3 m

When the shell diameter, D, is smaller, there are larger disparities between both heat transfer coefficients and pressure gradients obtained by using the two different models, and the disparities become smaller with increase of shell diameter, D. For the same shell diameter, D, of 0.3 m and different Reynolds numbers ranging from 6000-50000, h'/h varies between 1.36 and 1.41, $\Delta p'/\Delta p$ varies between 1.76 and 1.81, and $(h'/\Delta p')/(h/\Delta p)$ varies between 0.77 and 0.79. The fluctuations of all ratios of heat transfer coefficients, pressure gradients and heat transfer coefficient per unit pressure drop are all less than 4%. It is concluded that all ratios of heat transfer coefficients, pressure gradients and heat transfer coefficient per unit pressure drop are independent of Reynolds number for the same shell diameter.

To analyze the cause for the disparities between the computed results by the two adopted models, the convective heat transfer coefficients of tubes located in different positions in the shell side were studied. When the shell diameter, D, is 0.2 m, serial numbers of heat transfer tubes in the shell side are shown in fig. 7(a). When the Reynolds number is 10000, the convective heat transfer coefficients corresponding to tubes computed by using two different models

are compared in fig. 7(b). The results show that the convective heat transfer coefficients of tubes calculated using the PWCM are higher than that calculated using the PUDM. The differences become greater with the decrease of the distance to the shell axis.

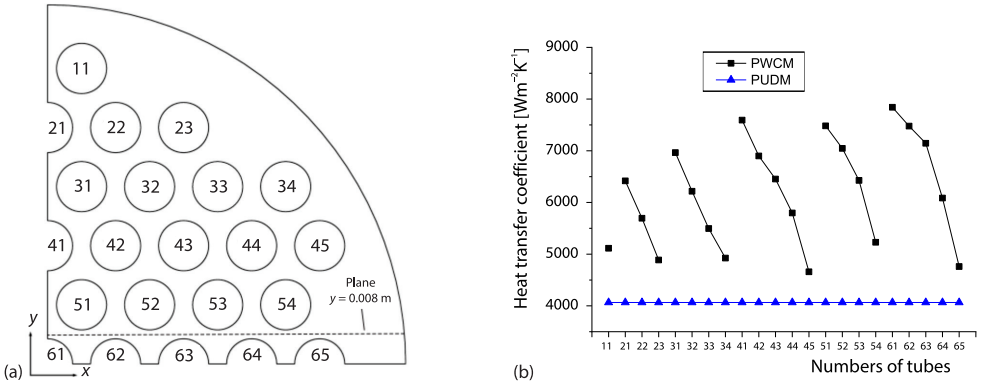

Figure 7. Convective heat transfer coefficients of different tubes; (a) number names of heat transfer tubes and (b) convective heat transfer coefficients

On the longitudinal section of $y = 0.008$ m shown in the fig. 7(a), the velocity contour of fluid-flow in shell side is shown in fig. 8(a). The fluid velocity distribution on the line *a* of fig. 8(a) is shown in fig. 8(b). Because of the effect of the shell wall and the block function of the support baffles, the fluid velocity is very small in the region near the shell wall, where a flow dead zone is formed. The fluid velocity increases with the decrease of the distance to the shell axis. The fluid velocity in the central region is higher than that near the shell, which results in a higher convective heat transfer coefficient for tubes in the central region than that near the shell. While in the PUDM, due to the fact that the influences of the inner wall of the shell and the edges of the support plates are ignored, the fluid velocity in the flow unit duct model is smaller than that in the main flow region in the PWCM, which results to smaller convective heat transfer coefficient and pressure gradient.

The larger the shell diameter, the smaller the ratio of the near-wall area to the total flow area. The influences of the shell wall and the edges of the support baffles on the flow is also smaller. The fluid velocity in the main flow region becomes closer to mean velocity, and the disparity between simulation results computed by using the two models gets smaller.

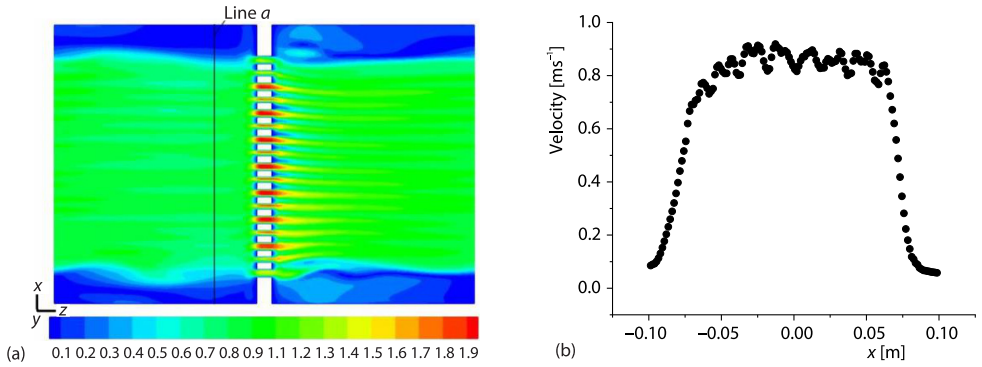

Figure 8. Velocity contour and distribution; (a) velocity contour on the cross-section. and (b) velocity distribution on the line *a*

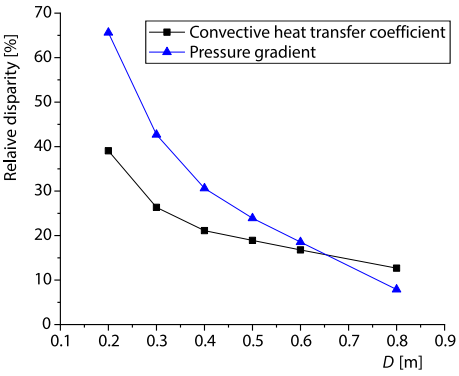

Figure 9. Relative disparities for the convective heat transfer coefficient and the pressure gradient

The relative disparities between the numerical results computed by using the PUDM and that by using the PWCM are shown in fig. 9. It demonstrates that the relative disparity decreases considerably with the increase of the shell diameter. When the shell diameter, D, is 0.8 m, the relative disparity of the convective heat transfer coefficient decreases to about 12.7%, and the relative disparity of pressure gradient reduces to 7.9%. It can be assumed that when the shell diameter is greater than 0.8 m, the PUDM can obtain results that meet the actual engineering requirements while consuming fewer computational resource.

Improved correlations for the PUDM

When the shell diameter is less than 0.8 m, the difference between the calculation results using the PUDM and those using the PWCM is significant. The results obtained by using the PWCM represent more the real situation with less simplification of structure. To extend the application of the PUDM, it is improved using the calculated results of the PWCM. The improved correlations for convective heat transfer coefficients and pressure gradients were derived using least squares and multiple linear regression:

$$P_{\mathrm{h}} = \frac{h'}{h} = 4.144\left(\frac{D}{d_{\mathrm{e}}}\right)^{-0.278}\left(\frac{L_{\mathrm{b}}}{d_{\mathrm{e}}}\right)^{-0.095} \tag{11}$$

$$P_{\Delta p} = \frac{\Delta p'}{\Delta p} = 15.09\left(\frac{D}{d_{\mathrm{e}}}\right)^{-0.706}\left(\frac{L_{\mathrm{b}}}{d_{\mathrm{e}}}\right)^{-0.032} \tag{12}$$

where P_{h} is heat transfer coefficient correction factor, $P_{\Delta p}$ – the pressure gradient correction factor, h – convective heat transfer coefficient of the PUDM, h' – convective heat transfer coefficient of the PWCM, Δp – pressure gradient of the PUDM, and $\Delta p'$ – pressure gradient of the PWCM. The correlations can be used for the design calculation of heat exchanger with trefoil-hole baffle and are applicable in the following ranges: Re = 6000-50000, D = 0.2-0.8 m, and L_{b} = 0.15-0.60 m.

With the correlations, the improved results by using the PUDM and the results by using the PWCM were compared, and the comparison results of the convective heat transfer coefficients and the pressure gradients are shown in fig. 10. The errors of corrections of convective heat transfer coefficients and pressure gradients are less than 10% and 15%, respectively.

The correlations also revealed quantitatively the effect of the shell wall and the edges of the support baffles on thermodynamics with the varying of shell diameter and baffle spacing. With the improved correlations for the condition of the shell diameter, D, smaller than 0.8 m, the convective heat transfer coefficients and pressure gradient can be obtained by using the PUDM to improve the computational efficiency.

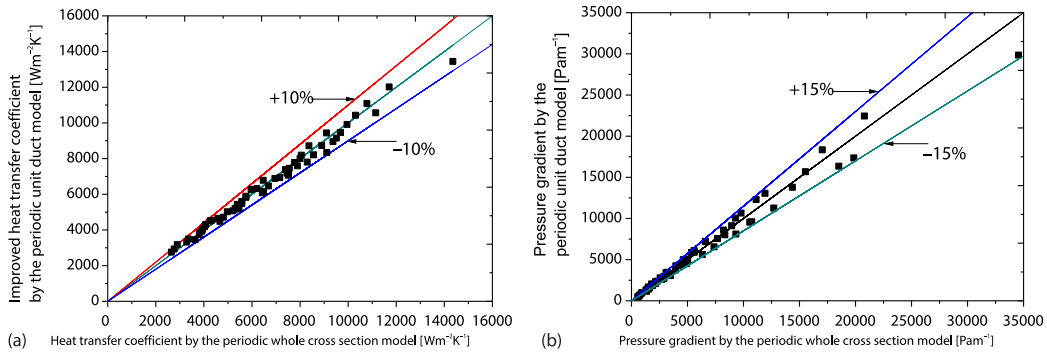

Figure 10. Errors of corrections for heat transfer coefficient and pressure gradient; (a) convective heat transfer coefficient and (b) pressure gradient

Conclusions

Both the PWCM and the PUDM can be adopted in the study on performances of the shell side for the heat exchangers with longitudinal fluid-flow in shell side. To evaluate the effects of the shell wall and the edges of the baffles on characteristics in the shell side and discuss the difference between the two numerical models applying to the same structure, two models for the shell side were built, and numerical calculations were performed. The suitability of the models and the influencing factors were discussed. The main conclusions are as follows.

- The fluid velocity at some points on the shell side was measured using the LDV system. The numerical simulated results matched well with the measured values. The validity and accuracy of the simulations are proved. The study methods and conclusions provide a reference for numerical modelling and improvement of STHX.
- Due to the effect of shell wall and baffles edges, the convective heat transfer coefficients and pressure gradients obtained with the PUDM are smaller than those obtained with the PWCM. And the ratios of heat transfer coefficient h'/h, pressure gradient $\Delta p'/\Delta p$ and heat transfer coefficient per unit pressure drop $(h'/\Delta p')/(h/\Delta p)$ are independent of Reynolds number. The difference between the results calculated using the two models decreases with increase of the shell diameter, D.
- When the shell diameter, D, is 0.8 m, the disparities between the computed results by using two models drop to about 10%. The influences of the shell wall and the edges of baffles on thermodynamics of shell side become weaker, and which can be ignored. When the shell diameter, D, is more than 0.8 m, numerical calculations can be carried out by adopting the PUDM to save computational resource.
- When the shell diameter, D, is smaller than 0.8 m, modified correlations of the convective heat transfer coefficient and pressure drop for the PUDM were proposed. The correlations also revealed quantitatively the effect of the shell wall and the edges of baffles on thermodynamics with the varying of shell diameter and baffle spacing.

Acknowledgment

This work was supported by the National Natural Science Foundation of China [Grant No. 51776190, 21776263].

Nomenclature

A – heat transfer area, [m^2]
c_p – specific heat capacity, [Jkg^{-1}K^{-1}]
D – inner diameter of shell, [m]
d_e – equivalent diameter of the shell side, [m]
d_o – diameter of tube, [m]
h – convective heat transfer coefficient of the PUDM, [Wm^{-2}K^{-1}]
h' – convective heat transfer coefficient of the PWCM, [Wm^{-2}K^{-1}]
L_b – baffle spacing, [m]
$\dot{m}$ – mass rate of flow, [kgs^{-1}]
P_t – tube pitch, [m]
P_h – heat transfer coefficient correction factor, [–]
$P_{\Delta p}$ – pressure gradient correction factor, [–]
p – pressure, [Pa]
Δp – pressure gradient of the PUDM, [Pam^{-1}]
$\Delta p'$ – pressure gradient of the PWCM, [Pam^{-1}]
Q – flow rate, [m^{3}h^{-1}]
Re – Reynolds number (=$\rho d_e U/\mu$), [–]
s – model length in periodic model, [m]
T – mean bulk temperature of fluid, [K]
T_w – temperature of tube wall, [K]
T_{in} – mean temperature of inlet fluid, [K]
T_{out} – mean temperature of outlet fluid, [K]
U – mean fluid velocity in the shell side, [ms^{-1}]
u, v, w – velocity components in the Cartesian co-ordinate system, [ms^{-1}]
x, y, z – co-ordinates in the Cartesian co-ordinate system, [m]

Greek symbols

Φ – outer diameter, [m]
λ – thermal conductivity, [Wm^{-1}K^{-1}]
ρ – density, [kgm^{-3}]
μ – dynamic viscosity, [kgm^{-1}s^{-1}]

References

[1] Abbas, A., *et al*., A Review of Correlations for Outside Boiling of Ammonia on Single Tube and Bundles, *Heat Transfer Engineering*, *39* (2018), 16, pp. 1425-1436
[2] Erdogan, A., Colpan, C. O., Performance Assessment of Shell and Tube Heat Exchanger Based Subcritical and Supercritical Organic Rankine Cycles, *Thermal Science*, *22* (2018), Suppl. 3, pp. S855-S866
[3] Geng, W., *et al.*, China's New Energy Development: Status, Constraints and Reforms, *Renewable & Sustainable Energy Reviews*, *53* (2016), Jan., pp. 885-896
[4] Kumaresan, G., *et al*., Numerical Analysis of Baffle Cut on Shell Side Heat Exchanger Performance with Inclined Baffles, *Heat Transfer Engineering*, *39* (2018), pp. 13-14, pp. 1156-1165
[5] Yang, J., Liu, W., Numerical Investigation on a Novel Shell-and-Tube Heat Exchanger with Plate Baffles and Experimental Validation, *Energy Conversion and Management*, *101* (2015), Sept., pp. 689-696
[6] You, Y., *et al.*, Experimental and Numerical Investigations of Shell-Side Thermo-Hydraulic Performances for Shell-and-Tube Heat Exchanger with Trefoil-Hole Baffles, *Applied Thermal Engineering*, *50* (2013), 1, pp. 950-956
[7] Gao, B., *et al*., Experimental Performance Comparison of Shell-Side Heat Transfer for Shell-and-Tube Heat Exchangers with Different Helical Baffles, *Heat Transfer Engineering*, *37* (2016), 18, pp. 1566-1578
[8] Milovancevic, U. M., *et al*., Thermoeconomic Analysis of Spiral Heat Exchanger with Constant Wall Temperature, *Thermal Science*, *23* (2019), 1, pp. 401-410
[9] Wang, X., *et al*., Numerical Analysis and Optimization Study on Shell-Side Performances of a Shell and Tube Heat Exchanger with Staggered Baffles, *International Journal of Heat and Mass Transfer*, *124* (2018), Sept., pp. 247-259
[10] Gu, X., *et al*., Heat Transfer and Flow Resistance Performance of Shutter Baffle Heat Exchanger with Triangle Tube Lay-out in Shell Side, *Advances in Mechanical Engineering*, *8* (2016), 3, 8
[11] Liu, J. J., *et al*., The 3-D Numerical Study on Shell Side Heat Transfer and Flow Characteristics of Rod-Baffle Heat Exchangers with Spirally Corrugated Tubes, *International Journal of Thermal Sciences*, *89* (2015), Mar., pp. 34-42
[12] Lei, Y., *et al*., Design and Performance Analysis of the Novel Shell-and-Tube Heat Exchangers with Louver Baffles, *Applied Thermal Engineering*, *125* (2017), Oct., pp. 870-879
[13] Heydari, A., *et al.*, Numerical Analysis of a Small Size Baffled Shell-and-Tube Heat Exchanger Using Different NanoFluids, *Heat Transfer Engineering*, *39* (2018), 2, pp. 141-153
[14] Bichkar, P., *et al*., Study of Shell and Tube Heat Exchanger with the Effect of Types of Baffles, *Procedia Manufacturing*, *20* (2018), Jan., pp. 195-200
[15] He, L., Li, P., Numerical Investigation on Double Tube-Pass Shell-and-Tube Heat Exchangers with Different Baffle Configurations, *Applied Thermal Engineering*, *143* (2018), Oct., pp. 561-569
[16] Zhu, L., *et al.*, Numerical Simulation on Shell Side Fluid-Flow and Heat Transfer in Heat Exchanger with Trefoil-Baffles, *CIESC Journal*, *65* (2014), 03, pp. 829-835

[17] Thanikodi, S., *et al*., Teaching Learning Optimization and Neural Network for the Effective Prediction of Heat Transfer Rates in Tube Heat Exchangers, *Thermal Science*, *24* (2020), 1, pp. 575-581
[18] Batalha Leoni, G., *et al.*, Assessment with Computational Fluid Dynamics of the Effects of Baffle Clearances on the Shell Side Flow in a Shell and Tube Heat Exchanger, *Applied Thermal Engineering*, *112* (2017), Feb., pp. 497-506
[19] Mellal, M., *et al*., Hydro-Thermal Shell-Side Performance Evaluation of a Shell and Tube Heat Exchanger under Different Baffle Arrangement and Orientation, *International Journal of Thermal Sciences*, *121* (2017), Nov., pp. 138-149
[20] Wang, K., *et al*., Flow Dead Zone Analysis and Structure Optimization for the Trefoil-Baffle Heat Exchanger, *International Journal of Thermal Sciences*, *140* (2019), June, pp. 127-134
[21] You, Y*., et al.*, Numerical Simulation and Performance Improvement for a Small Size Shell-and-Tube Heat Exchanger with Trefoil-Hole Baffles*, Applied Thermal Engineering*, *89* (2015), Oct., pp. 220-228
[22] El Maakoul, A., *et al*., Numerical Comparison of Shell-Side Performance for Shell and Tube Heat Exchangers with Trefoil-Hole, Helical and Segmental Baffles, *Applied Thermal Engineering*, *109* (2016), Part A, pp. 175-185
[23] Zhou, G., *et al*., A Numerical Study on the Shell-Side Turbulent Heat Transfer Enhancement of Shell-and-Tube Heat Exchanger with Trefoil-Hole Baffles, *Energy Procedia*, *75* (2015), Aug., pp. 3174-3179
[24] Ma, L., *et al.*, Numerical Study on Performances of Shell-Side in Trefoil-Hole and Quatrefoil-Hole Baffle Heat Exchangers, *Applied Thermal Engineering*, *123* (2017), Aug., pp. 1444-1455
[25] Dong, Q. W., *et al.*, Numerical and Experimental Investigation of Shellside Characteristics for ROD Baffle Heat Exchanger, *Applied Thermal Engineering*, *28* (2008), 7, pp. 651-660
[26] Rad, S. E., *et al*., Heat Transfer Enhancement in Shell-and-Tube Heat Exchangers Using Porous Media, *Heat Transfer Engineering*, *36* (2015), 3, pp. 262-277
[27] You, Y. H., *et al*., Full Model Simulation of Shellside Thermal Augmentation of Small Heat Exchanger with Two Tube Passes, *Heat Transfer Engineering*, *39* (2018), 12, pp. 1024-1035
[28] Dong, Q. W., Liu, M. S., *Heat Exchanger with Longitudinal Flow of Shellside Fluid* (in Chinese), Chemical Industry Press, Beijing, China, 2007
[29] Wang, Y., *et al*., Characteristics of Heat Transfer for Tube Banks in Crossflow and Its Relation with That in Shell-and-Tube Heat Exchangers, *International Journal of Heat and Mass Transfer*, *93* (2016), Feb., pp. 584-594
[30] Li, H., Kottke, V., Analysis of Local Shellside Heat and Mass Transfer in the Shell-and-tube Heat Exchanger with Disc-and-Doughnut Baffles, *International Journal of Heat and Mass Transfer*, *42* (1999), 18, pp. 3509-3521
[31] Yang, S., *et al*., Influence of Baffle Configurations on Flow and Heat Transfer Characteristics of Unilateral Type Helical Baffle Heat Exchangers, *Applied Thermal Engineering*, *133* (2018), Mar., pp. 739-748
[32] Wang, Y., *et al*., Characteristics of Fluid-Flow and Heat Transfer in Shellside of Heat Exchangers with Longitudinal Flow of Shellside Fluid with Different Supporting Structures, in: *Challenges of Power Engineering and Environment*, Int. Con. on Power Engineering, Hangzhou, China, 2007, pp. 474-479
[33] ***, Ansys Inc., FLUENT user's guide. Ansys Inc., 2018
[34] Wesseling, P., *Principles of Computational Fluid Dynamics*, Springer, Berlin, Germany, 2001
[35] Rothberg, S. J., *et al.*, An International Review of Laser Doppler Vibrometry: Making Light Work of Vibration Measurement, *Optics and Lasers in Engineering*, *99* (2017), Dec., pp. 11-22
[36] Xiong, J., *et al*., Experimental Investigation on Anisotropic Turbulent Flow in a 6×6 Rod Bundle with LDV, *Nuclear Engineering and Design*, *278* (2014), Oct., pp. 333-343
[37] Holman, J. P., *Heat Transfer*, McGraw-Hill, New York, USA, 2010

Paper submitted: November 6, 2021
Paper revised: January 21, 2022
Paper accepted: January 25, 2022